# The extraordinary structural evolution of massive galaxies

Szomoru, D.

CHAPTER 2

# CONFIRMATION OF THE COMPACTNESS OF A Z = 1.91 QUIESCENT GALAXY WITH HST/WFC3

We present very deep WFC3 photometry of a massive, compact galaxy located in the HUDF. This quiescent galaxy has a spectroscopic redshift $z = 1.91$ and has been identified as an extremely compact galaxy by Daddi et al. (2005). We use new $H_{\rm F160W}$ imaging data obtained with HST/WFC3 to measure the deconvolved surface brightness profile to $H \approx 28$ mag arcsec$^{-2}$. We find that the surface brightness profile is well approximated by a $n = 3.7$ Sérsic profile. Our deconvolved profile is constructed by a new technique which corrects the best-fit Sérsic profile with the residual of the fit to the observed image. This allows for galaxy profiles which deviate from a Sérsic profile. We determine the effective radius of this galaxy: $r_e = 0.42 \pm 0.14$ kpc in the observed $H_{\rm F160W}$-band. We show that this result is robust to deviations from the Sérsic model used in the fit. We test the sensitivity of our analysis to faint ``wings'' in the profile using simulated galaxy images consisting of a bright compact component and a faint extended component. We find that due to the combination of the WFC3 imaging depth and our method's sensitivity to extended faint emission we can accurately trace the intrinsic surface brightness profile, and that we can therefore confidently rule out the existence of a faint extended envelope around the observed galaxy down to our surface brightness limit. These results confirm that the galaxy lies a factor $\sim 10$ off from the local mass-size relation.

Daniel Szomoru, Marijn Franx, Pieter G. van Dokkum, Michele Trenti, Garth D. Illingworth, Ivo Labbé, Rychard J. Bouwens, Pascal A. Oesch, C. Marcella Carollo
*The Astrophysical Journal*, **714**, L244-L248, 2010

## 2.1 INTRODUCTION

A significant fraction of massive galaxies at $z \approx 2$ are early-type galaxies containing quiescent stellar populations (e.g., Franx et al. 2003; Daddi et al. 2005; Kriek et al. 2006). These galaxies must have formed very early in the universe's history and can therefore provide important constraints on galaxy formation and evolution models. Many of these quiescent galaxies have been found to be extremely compact, with effective radii a factor $\sim 6$ smaller than their low-z counterparts (e.g., Daddi et al. 2005; Trujillo et al. 2006; van Dokkum et al. 2008). This is quite puzzling, since these compact galaxies are passively evolving and are therefore not expected to change strongly in size or mass if they do not merge. We note that Mancini et al. (2010) find some large massive quiescent galaxies at $z \sim 1.5$, showing that not all massive quiescent galaxies at high redshift are compact.

Within the context of current models, galaxy mergers play an important role in galaxy evolution (e.g., White & Frenk 1991). These mergers may cause compact $z \sim 2$ galaxies to grow ``inside-out'', i.e., the mergers would increase the size of the galaxies (e.g., van Dokkum et al. 2010; Hopkins et al. 2009b). Whether the resulting size growth is large enough, however, is uncertain (e.g., Bezanson et al. 2009).

Several authors have emphasised that there are several systematic uncertainties that affect both radius and mass determinations. Firstly, effective radii may be underestimated due to complex morphologies. Specifically, an extended low surface brightness component could remain undetected due to low signal-to-noise (S/N), thereby lowering the observed size (e.g., Hopkins et al. 2009a; Mancini et al. 2010, but see van Dokkum et al. 2008; van der Wel et al. 2008). Secondly, mass-to-light gradients may result in a luminosity-weighted effective radius that is smaller than the mass-weighted effective radius (e.g., Hopkins et al. 2009a; Hopkins et al. 2009b). Such gradients arise in certain models for the formation of massive ellipticals (e.g., Robertson et al. 2006; Naab et al. 2007). Lastly, the inferred stellar masses may be affected by incorrect assumptions regarding the initial mass function (IMF) and stellar evolution models (e.g., Muzzin et al. 2009, and references therein).

In this Letter we use new very deep near-infrared (NIR) imaging data from the Hubble Space Telescope's Wide Field Camera 3 (HST/WFC3) to investigate the possibility of size underestimation due to lack of S/N. We examine the possibility of a ``hidden'' faint extended component being present in $z \approx 2$ compact quiescent galaxies, focusing on the most massive quiescent galaxy in the Hubble Ultra Deep Field (HUDF), which has previously been studied by Daddi et al. (2005). We adopt the following values for cosmological parameters: $H_0 = 70$ km s$^{-1}$ Mpc$^{-1}$, $\Omega_m = 0.3$, and $\Omega_\Lambda = 0.7$. All stellar masses are derived assuming a Kroupa IMF (Kroupa, 2001). All effective radii are circularized, unless noted otherwise.

## 2.2 OBSERVATIONS AND SAMPLE

Our study utilises new WFC3/IR $H_{\rm F160W}$-band imaging data taken within the HUDF. This data is part of the first of three ultra-deep pointings which will be completed over the next year as part of the HUDF09 HST Treasury program (GO11563). The current WFC3 imaging consists of 78600 seconds of exposure time in the $H_{\rm F160W}$ band, leading to a limiting magnitude of 28.8. The PSF FWHM is $\sim 0.16$ arcsec. Details of the data reduction can be found in Bouwens et al. (2010).

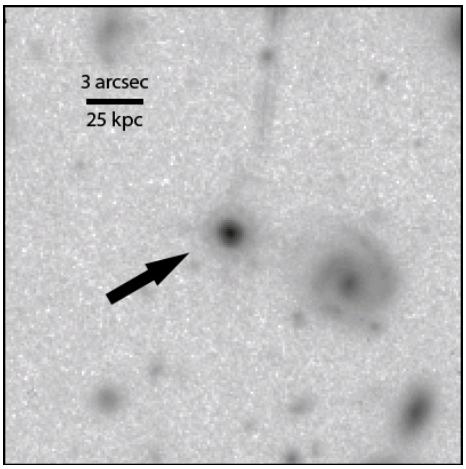


Figure 2.1: The WFC3 $H_{\rm F160W}$-band image of the galaxy. It is well-separated from its nearest neighbors.

Since the WFC3 data does not cover the complete HUDF, most of the compact massive $z \approx 2$ galaxies from e.g. Daddi et al. (2005) and Cimatti et al. (2008) fall outside of the observed area. From the compact $z \approx 2$ galaxies inside the WFC3 HUDF image area we select the most massive one, located at $\alpha = 3:32:38.12$, $\delta = -27:47:49.63$. This galaxy has a spectroscopic redshift $z = 1.91$ (Daddi et al., 2005), stellar mass $M_* = 0.56 \times 10^{11} M_\odot$ (Wuyts et al. 2008; Förster Schreiber et al. 2009), and effective radius $r_e < 1$ kpc in the observed $z$ band (Daddi et al. 2005; Cimatti et al. 2008). It was identified by Daddi et al. (2005) as passively evolving based on the $BzK$ criterion. A summary of the galaxy's structural parameters is given in Table 2.1. An image of the galaxy is shown in Figure 2.1. It is sufficiently separated from its neighbors to prevent contamination of its surface brightness profile.

## 2.3 FITTING AND SIZE

We use the GALFIT package (Peng et al., 2002) to fit two-dimensional Sérsic (1968) model profiles convolved with the PSF to the observed surface brightness distribution. This is an essential step in deriving the structure of the galaxy, as the FWHM of the PSF of the WFC3 images is significant compared to the size of the galaxy. We use a PSF extracted from a nearby unsaturated star and base our masking image on a SExtractor (Bertin & Arnouts 1996) segmentation map. We fit nine different models with fixed Sérsic index ($n = 1, 2, ..., 9$), as well as a model where $n$ is a free parameter.

The effective radii from the Sérsic fits range between 0.42 and 0.48 for Sérsic indices varying between $n = 1$ and $n = 9$, with the free-$n$ fit producing a value of 0.43 kpc (at $n = 3.7$). The best-fit Sérsic profiles are shown in Figure 2.2. Despite the fact that the effective radii are rather similar, it is clear that the derived profiles vary significantly with $n$.

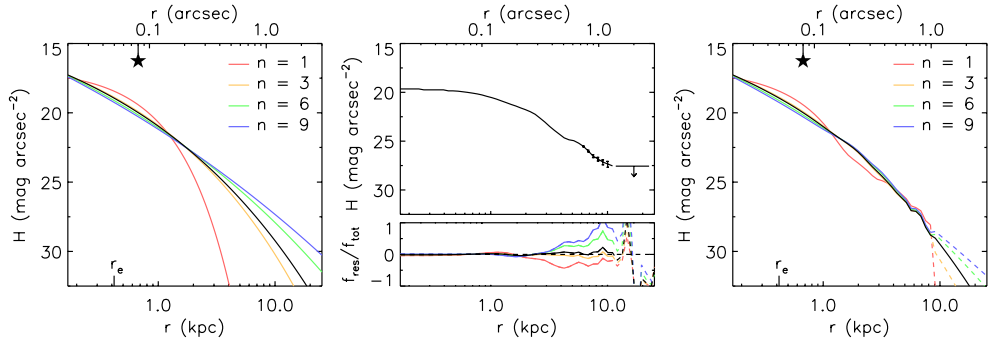


Figure 2.2: Our method of correcting the observed surface brightness profile for the effects of the HST WFC3 PSF and incorrect profile modeling. In the left panel the best-fitting Sérsic models, derived from a 2D fit using a star as the PSF, are shown for different values of n. The black curve indicates the free-$n$ fit, with $n = 3.7$. The profiles show large variations. In the top center panel the observed profile is shown. The residual fluxes from the Sérsic fits are shown in the bottom panel as a fraction of the observed flux. In the right panel the profiles derived using our ``residual-correction'' method are shown. At large radii, where uncertainties in the sky determination become significant, the profile is extrapolated. This is indicated by dashed curves. The residual-corrected profiles are much more robust to modeling errors than the uncorrected profiles. The derived effective radius is indicated on the bottom x-axis, the PSF size (HWHM) is indicated by the star symbol on the top x-axis. The solid horizontal line in the middle panel indicates the $3\sigma$ sky noise level. As can be seen, the surface brightness profile can be robustly measured to a surface brightness of 28 mag arcsec$^{-2}$.

There is no intrinsic reason why galaxies should have ``perfect'' Sérsic profiles. Although locally the surface brightness profiles of elliptical galaxies are well fitted by single Sérsic profiles over a large range of radii (e.g., Kormendy et al. 2009), at high redshift very few radial profiles have been measured directly; in most cases PSF-convolved model fits have been performed to the imaging. Moreover, if elliptical galaxies grow by an inside-out process (e.g., Hopkins et al. 2009a; Feldmann et al. 2009), the surface brightness profiles of their progenitors may deviate from Sérsic profiles. We therefore developed a method to derive more robust intensity profiles, which depend less on the Sérsic $n$ parameter used for the fit.

Our approach is the following: for each Sérsic fit, we calculate the residual image, which is an image of the observed flux minus the PSF-convolved model. We derive a profile of the residual flux measured along circles centered on the galaxy. We add this residual profile to the deconvolved model Sérsic profile. We note that the intrinsic profile is deconvolved for PSF, but the residuals are not. This procedure is similar to how the CLEAN deconvolution method employed in radioastronomy handles residuals (Högbom, 1974). We thus remove or add flux at those radii where the model does not adequately describe the data, making a first order correction for errors caused by the incorrect profile choice. For large radii, where (systematic) uncertainties in the sky determination become significant, we extrapolate the residual-corrected profile by using the uncorrected Sérsic profile, scaled to the residual-corrected profile at the transition radius. These ``residual-corrected'' profiles are then integrated in order to determine the true half-light radius, which we refer to as

Table 2.1: Structural parameters

| Source | $n$ | $r_e$ (kpc) | $b/a$ | $M_*$ ($10^{11} M_\odot$) | $H^{tot}_{\rm F160W}$ (AB) |
|---|---|---|---|---|---|
| This Letter | $3.7 \pm 0.38$ | $0.42 \pm 0.14$ | 0.70 | ... | $22.15 \pm 0.067$ |
| Previous work | $4.7 \pm 0.6$[1] | $0.79 \pm 0.08$[1] | 0.74[1] | 0.56[2] | $22.12 \pm 0.03$[2] |

[1]Daddi et al. (2005), measured in $z_{\rm F850LP}$ band

[2]Wuyts et al. (2008)

$r_{e,deconv}$. The residual-corrected profiles are shown in Figure 2.2. The structural parameters of the best-fitting profile are given in Table 2.1.

It is clear from Figure 2.2 that the residual-corrected profiles are much less sensitive to the Sérsic-$n$ value adopted for the initial modeling, especially at radii beyond a few kpc. Furthermore, deviations from the Sérsic profile are taken into account; as we show in Section 4, using the residual-corrected profile we can trace the true surface brightness profile much more accurately than using simple analytical Sérsic fits. This is due to the fact that the S/N of the faint emission at large radii is so low that the fitting procedure ignores it, even though a lot of flux can originate there. Thus the stability of the parameters derived from Sérsic fits is no guarantee for correctness. This is particularly relevant when the galaxies have complex morphologies, such as in the case of a bright, compact galaxy surrounded by a faint, extended envelope.

Uncertainties in $r_{e,deconv}$ and the total $H$-band magnitude are estimated from the range in values obtained from the fixed-$n$ residual-corrected profiles. The errors given in Table 2.1 are the rms errors of the best-fit parameters from all of the fits, and give an indication of the systematic errors due to differences between the observed surface brightness profile and the Sérsic models used in the fitting procedure. The uncertainty in $n$ is estimated using simulations: we add random sky noise to the observed galaxy image. This is repeated several times, resulting in a number of images, on each of which we perform the fitting procedure described above. The uncertainty given in Table 2.1 is two times the rms error of the best-fit parameter from all of the fits.

Our results are the following: the galaxy is best fit by a Sérsic profile with $n = 3.7$. Using the residual-corrected profile we find that the effective radius of the galaxy is $r_{e,deconv} = 0.050$ arcsec, which corresponds to $r_{e,deconv} = 0.42$ kpc. If we fix the Sérsic index to a constant value, the inferred size does not vary substantially: $r_{e,deconv}$ varies from 0.31 kpc for $n = 9$ to 0.51 kpc for $n = 1$. Thus, the deviations from the best-fitting profile are $< 20\%$. Our size estimate is therefore reasonably robust to deviations from the model profile.

We have investigated the influence of PSF uncertainties; if we use PSFs extracted from other stars in the field we find variations in $r_{e,deconv}$ of $< 10\%$. We have used the Tiny Tim software package[1] to investigate the spatial dependence of the PSF independently. We

[1]`http://www.stsci.edu/software/tinytim`

find that the derived effective radius changes very little with the position of the reference star used, with a maximum of 10% in opposite corners of the field. The difference in effective radius due to the distance between the reference star and the galaxy is less than 1%. We therefore conclude that PSF errors do not present a significant problem in our analysis.

## 2.4 LOW SURFACE BRIGHTNESS SENSITIVITY

We now determine whether faint extended emission would be detected using our data. To this end we construct several simulated galaxy images which consist of two components; a compact component, described by a $n = 4$ Sérsic profile with an effective radius roughly equal to the observed galaxy (see Table 2.1), and an extended component, described by a Sérsic profile with either $n = 4$, $r_e \approx 3.5$ kpc or $n = 1$, $r_e \approx 15$ kpc. The extended component has a flux that is either 10% or 50% of the compact component's flux. The compact component's flux is chosen such that the total flux of the two components is equal to the observed galaxy's total flux. The images are convolved with the PSF, and sky and readout noise are added. The images are then fit with a single Sérsic profile using GALFIT, and a residual-corrected profile is constructed. By comparing the half-light radii obtained in this way to the intrinsic half-light radii we can quantify the sensitivity of our data to low surface brightness components.

The results of our simulated galaxy fits are shown in Figure 2.3. The residual-corrected profiles closely follow the intrinsic profiles. The effective radii derived from the residual-corrected profiles are very close to the intrinsic effective radii: in three of the cases the difference is less than 5%. For the $n = 1$ extended component with a total flux equal to half of the compact component's flux the inferred radius is 10% smaller than the intrinsic radius, comparable to the systematic error due to modeling uncertainties (see Section 2.3). We also tested $n = 4$ and $n = 1$ models with effective radii of several kpc for the $n = 1$ extended component: these models are so well approximated by Sérsic models with higher values of $n$ ($> 4$) that normal Sérsic profile fitting immediately retrieves the correct effective radii.

In conclusion, our method used on these deep data is sensitive to a faint extended component down to a surface brightness of $H \approx 28$ mag arcsec$^{-2}$, and using our method we retrieve effective radii that are within $1\sigma$ of the true value. We note that the effective radii obtained using the conventional method are, in most cases, very close to the intrinsic effective radii. However, the surface brightness profiles obtained in this way clearly deviate from the intrinsic profiles.

## 2.5 DISCUSSION

We have found that the galaxy under consideration is indeed remarkably small. We have fitted a Sérsic model to the observed flux distribution, and corrected the profile for the observed deviations. We have measured the galaxy's half light radius: $r_{e,deconv} = 0.42 \pm 0.14$ kpc. This result is robust to changes in the imposed Sérsic profile. As a check of our data's

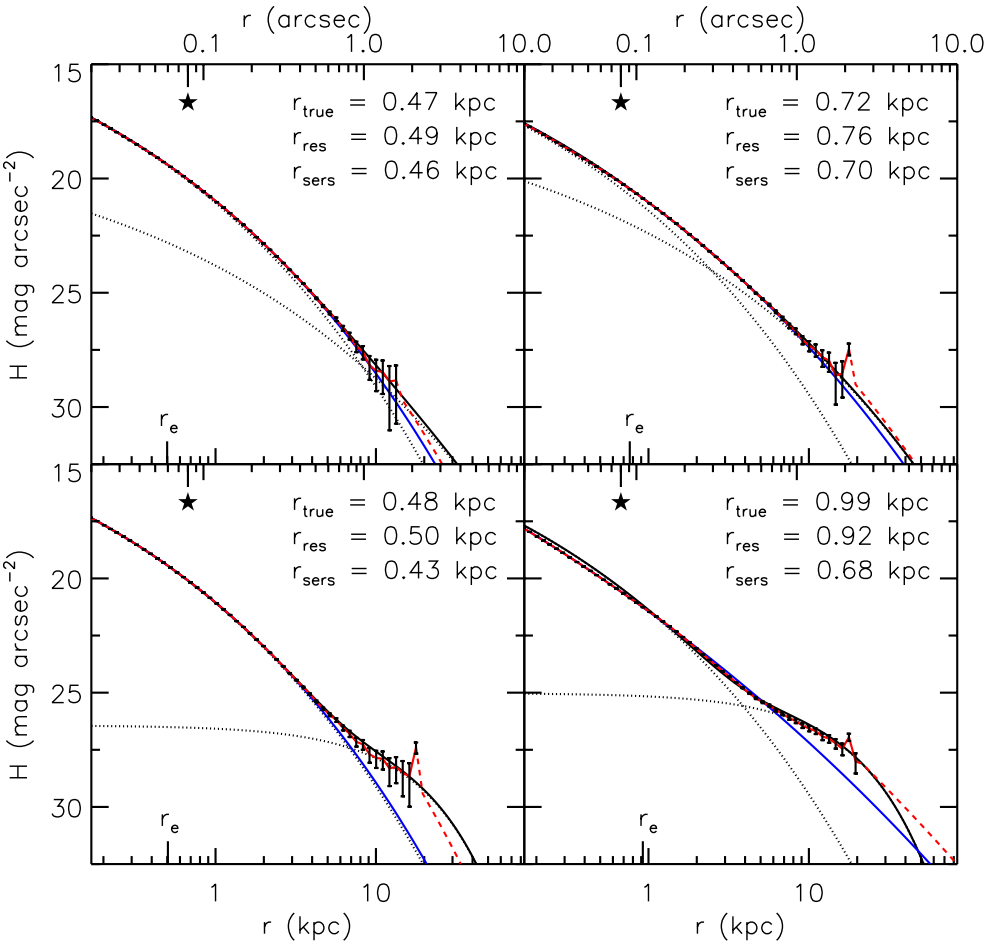


Figure 2.3: Residual-corrected fits to simulated galaxy images (red curves). *Top:* compact $n = 4$ profile and extended $n = 4$ profile, with flux ratios $10 : 1$ (*left*) and $2 : 1$ (*right*). *Bottom:* compact $n = 4$ profile and extended $n = 1$ profile, with the same flux ratios as in the top panels. At large radii, where uncertainties in the sky determination become significant, the profile is extrapolated. This is indicated by dashed curves. The solid black curves indicate the total intrinsic surface brightness profiles, the dotted black curves indicate the individual components that make up these profiles. The best-fit uncorrected Sérsic profiles are shown as blue curves. These deviate strongly from the true profiles at large radii. The residual-corrected profiles (red curves) follow the intrinsic profiles extremely well, demonstrating that our method recovers the intrinsic profiles accurately; the derived effective radii, indicated on the bottom x-axes, are within 10% of the true effective radii. The PSF size (HWHM) is indicated by the star symbols on the top x-axes.

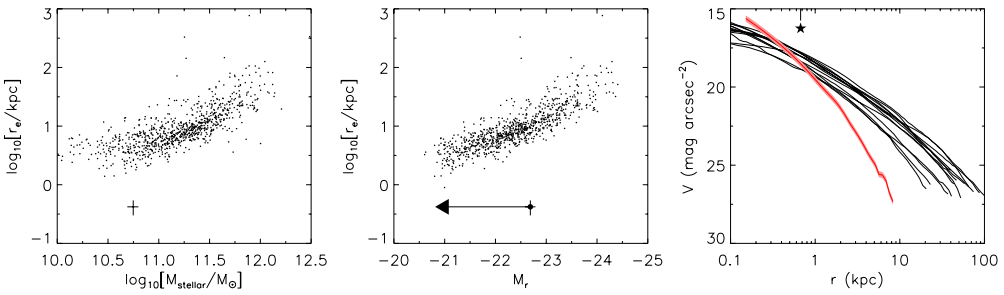


Figure 2.4: Relations between size and stellar mass (*left*) and size and rest-frame $r$-band luminosity (*middle*) for a sample of low-redshift galaxies, taken from Guo et al. (2009). The large symbol with error bars indicates the position of our galaxy. Low-redshift galaxies are much larger at similar stellar masses and luminosities. The arrow in the middle plot indicates the change in luminosity due to passive evolution to $z = 0$. The size of the galaxy is smaller than the local equivalents by a factor of 10. *Right:* comparison of best-fit residual-corrected rest-frame V-band surface brightness profile to elliptical galaxies in the Virgo cluster, from Kormendy et al. (2009). Virgo galaxies are plotted in different colors, corresponding to the following mass bins: black: $M_*/M_\odot > 10^{11}$; blue: $10^{10} < M_*/M_\odot < 10^{11}$. The observed high-$z$ surface brightness profile has been corrected for cosmological surface dimming and passive M/L evolution from $z = 1.91$ to $z = 0$ (see text). Assuming the galaxy has a mass $> 10^{11} M_\odot$ at $z = 0$ its profile at large radii will evolve very strongly over the next 10 Gyr. The central surface brightness profile, on the other hand, shows much less evolution between $z \approx 2$ and $z = 0$.

sensitivity to a low surface brightness component we have constructed simulated galaxy images which include a faint extended component. We can reproduce the effective radii to 10% using our technique.

A possible cause for concern is that the galaxy might deviate strongly from a Sérsic profile. We have incorporated the residuals in our fit to compensate for such errors, and we note that the residuals from our best Sérsic model fit are quite low ($< 10\%$). This implies that our model profile is close to the real profile. This, and the fact that varying $n$ has little influence on the derived half-light radius, suggests that our results are not strongly affected by this source of error.

Thus, our findings indicate that the small effective radius that has been found is not due to oversimplified modeling or a lack of S/N, and gives additional evidence that a strong evolution in size occurs from $z \approx 2$ to $z = 0$. It should be noted that our derived effective radius is 1.6 times smaller than the radii derived by Daddi et al. (2005) in the $i$ and $z$ bands. When we repeat our analysis on the ACS $z$-band data we obtain a slightly different value, $r_{e,deconv} \approx 0.65$ kpc (uncircularized), closer to the deep $H$-band imaging, and somewhat smaller than the value derived by Daddi et al. (2005) (but consistent within the errors). Hence all bands indicate a very small size.

Figure 2.4 illustrates the difference in size and mass between our galaxy and the $z = 0$ elliptical population; plotted in the first two panels are the compact galaxy we have studied and a sample of low-redshift central galaxies from groups and clusters in the Sloan Digital Sky Survey, analyzed by Guo et al. (2009). The compact $z \approx 2$ galaxy lies far off from

the $z = 0$ mass-size relation. The middle panel shows the galaxy on the mass-luminosity relation. We estimated the luminosity evolution of the compact galaxy from $z = 1.91$ to $z = 0$ in two ways: we first used the rest-frame $B - I$ color difference between low and high redshift to estimate the difference in mass-to-light ratio. Second we used the Fundamental Plane to estimate the evolution from $z = 0$ to $z = 1$ from van der Wel et al. (2005), and used the average evolution of the mass-to-light ratios of early-types in the CDFS at $z = 1$ and the $z = 1.91$ galaxy, both from Förster Schreiber et al. (in preparation). The resulting evolution is 1.8-2.2 magnitudes. As a result, the galaxy still lies off from the size-magnitude relation after correcting for evolution.

In the third panel of Figure 2.4 we compare the surface brightness profile of this galaxy to those of elliptical galaxies in the Virgo cluster. The profile shown has been corrected for cosmological surface brightness dimming and passive luminosity evolution from $z = 1.91$ to $z = 0$. The total correction is $-3.5 + 2 \approx -1.5$ magnitudes. Even though the galaxy has an average density $> 100$ times larger than the average $z = 0$ elliptical of the same mass, its surface brightness profile in the central kpc is actually rather similar to those of the most massive galaxies at $z = 0$ - the average density measured at fixed physical radius is not that different. This is consistent with results obtained by other authors (e.g., Bezanson et al. 2009; Hopkins et al. 2009a; Feldmann et al. 2009; van Dokkum et al. 2010). Thus, the main difference between $z = 0$ and this $z \approx 2$ galaxy is at larger radii where the $z \approx 2$ galaxy has much lower surface brightness. Such a result could be explained by inside-out growth.

We note also that there may be significant errors in the mass determination of $z \approx 2$ compact galaxies, due to e.g. incorrect assumptions about the IMF. Changes in the low mass end of the IMF affect both the masses of the high redshift and low redshift galaxies, and are nearly irrelevant. However, changes in the slope of the IMF will affect the derived passive evolution between $z = 2$ and $z = 0$, and will increase or decrease the size evolution. Changes in the IMF could thus have important consequences for evolution. Future deep NIR spectroscopic data should provide direct information on the kinematics of these objects and will allow us to confirm their high masses (see e.g., van Dokkum et al. 2009).

Finally, it will be interesting to obtain similar deep data on other compact massive galaxies, so that their profiles can be analyzed to the same surface brightness limit. We note that stacking can also lead to a great increase in imaging depth; e.g., Cassata et al. (2009), van Dokkum et al. (2008), and van der Wel et al. (2008) stack samples of compact galaxies and obtain very good constraints on their average surface brightness profile. However, with the new WFC3 data available in the coming years many more compact massive galaxies can be studied on an individual basis.

## REFERENCES


Beckwith, S. V. W., Stiavelli, M., Koekemoer, A. M., Caldwell, J. A. R., Ferguson, H. C., Hook, R., Lucas, R. A., Bergeron, L. E., Corbin, M., Jogee, S., Panagia, N., Robberto, M., Royle, P., Somerville, R. S., Sosey, M. 2006, AJ, 132, 1729

Bertin, E., Arnouts, S. 1996, A&AS, 117, 393

Bezanson, R., van Dokkum, P. G., Tal, T., Marchesini, D., Kriek, M., Franx, M., Coppi, P. 2009, ApJ, 697, 1290

Bouwens, R. J., Illingworth, G. D., Oesch, P. A., Stiavelli, M., van Dokkum, P. G., Trenti, M., Magee, D., Labbé, I., Franx, M., Carollo, C. M. 2010, ApJ, 709, L133

Cassata, P., Giavalisco, M., Guo, Y., Ferguson, H., Koekemoer, A., Renzini, A., Fontana, A., Salimbeni, S., Dickinson, M., Casertano, S., Conselice, C. J., Grogin, N., Lotz, J. M., Papovich, C., Lucas, R. A., Straughn, A., Gardner, J. P., Moustakas, L. 2009, arXiv:0911.1158

Cimatti, A., Cassata, P., Pozzetti, L., Kurk, J., Mignoli, M., Renzini, A., Daddi, E., Bolzonella, M., Brusa, M., Rodighiero, G., Dickinson, M., Franceschini, A., Zamorani, G., Berta, S., Rosati, P., Halliday, C. 2008, A&A, 482, 21

Daddi, E., Renzini, A., Pirzkal, N., Cimatti, A., Malhotra, S., Stiavelli, M., Xu, C., Pasquali, A., Rhoads, J. E., Brusa, M., di Serego Alighieri, S., Ferguson, H. C., Koekemoer, A. M., Moustakas, L. A., Panagia, N., Windhorst, R. A. 2005, ApJ, 626, 680

van Dokkum, P. G. 2005, ApJ, 130, 2647

van Dokkum, P. G., Franx, M., Kriek, M., Holden, B., Illingworth, G. D., Magee, D., Bouwens, R., Marchesini, D., Quadri, R., Rudnick, G., Taylor, E. N., Toft, S. 2008, ApJ, 677, L5

van Dokkum, P. G., Whitaker, K. R., Brammer, G., Franx, M., Kriek, M., Labbé, I., Marchesini, D., Quadri, R., Bezanson, R., Illingworth, G. D., Muzzin, A., Rudnick, G., Tal, T., Wake, D. 2010, ApJ, 709, 1018

van Dokkum, P. G., Kriek, M., Franx, M. 2009, Nature, 460, 717

Eggen, O. J., Lynden-Bell, D., Sandage, A. R. 1962, ApJ, 136, 748

Feldmann, R., Carollo, C. M., Mayer, L., Renzini, A., Lake, G., Quinn, T., Stinson, G. S., Yepes, G. 2009, ApJ, 709, 218

Franx, M., Labbé, I., Rudnick, G., van Dokkum P. G., Daddi, E., Förster Schreiber, N. M., Moorwood, A., Rix, H.-W., Röttgering, H., van de Wel, A., van der Werf, P., van Starkenburg, L. 2003, ApJ, 587, L79

Guo, Y., McIntosh, D. H., Mo, H. J., Katz, N., van den Bosch, F. C., Weinberg, M., Weinmann, S. M., Pasquali, A., Yang, X. 2009, MNRAS, 398, 1129

Högbom, J. A. 1974, A&AS, 15, 417

Hopkins, P. F., Bundy, K., Murray, N., Quataert, E., Lauer, T. R., Ma, C.-P. 2009a, MNRAS, 398, 898

Hopkins, P. F., Bundy, K., Hernquist, L., Wuyts, S., Cox, T. J. 2009b, MNRAS, 401, 1099

Kormendy, J., Fisher, D. B., Cornell, M. E., Bender, R. 2009, ApJS, 182, 216

Kriek, M., van Dokkum, P. G., Franx, M., Quadri, R., Gawiser, E., Herrera, D., Illingworth, G. D., Labbé, I., Lira, P., Marchesini, D., Rix, H.-W., Rudnick, G., Taylor, E. N., Toft, S., Urry, M. C., Wuyts, S. 2006, ApJ, 649, 71

Kroupa, P. 2001, MNRAS, 322, 231

Mancini, C., Daddi, E., Renzini, A., Salmi, F., McCracken, H. J., Cimatti, A., Onodera, M., Salvato, M., Koekemoer, A. M., Aussel, H., Le Floc'h, E., Willott, C., Capak, P. 2010, MNRAS, 401, 933

Muzzin, A., van Dokkum, P. G., Franx, M., Marchesini, D., Kriek, M., Labbé, I. 2009, ApJ, 706, L188

Naab, T., Johansson, P. H., Ostriker, J. P., Efstathiou, G. 2007, ApJ, 658, 710

Peng, C. Y., Ho, L. C., Impey, C. D., Rix, H.-W. 2000, AJ, 124, 266

Robertson, B., Bullock, J. S., Cox, T. J., Di Matteo, T., Hernquist, L., Springel, V., Yoshida, N. 2006, ApJ, 645, 986

Sérsic, J. L. 1968, Atlas de Galaxias Australes (Cordoba: Obs. Astron.)

Trujillo, I., Feulner, G., Goranova, Y., Hopp, U., Longhetti, M., Saracco, P., Bender, R., Braito, V., Della Ceca, R., Drory, N., Mannucci, F., Severgnini, P. 2006, MNRAS, 373, L36

van der Wel, A., Franx, M., van Dokkum, P. G., Rix, H.-W., Illingworth, G. D., Rosati, P. 2005, ApJ, 631, 145

van der Wel, A., Holden, B. P., Zirm, A. W., Franx, M., Rettura, A., Illingworth, G. D., Ford, H. C. 2008, ApJ, 688, 48

White, S. D. M., Frenk, C. S. 1991, ApJ, 379, 52

Wuyts, S., Labbé, I., Förster Schreiber, N. M., Franx, M., Rudnick, G., Brammer, G. B., van Dokkum, P. G. 2008, ApJ, 682, 985